


Anomalous diffusion in a bench-scale pulsed fluidized bedJonathan E. Higham *University of Liverpool, School of Environmental Sciences, Department of Geography and Planning, Roxby Building, Liverpool, L69 7ZT, United Kingdom*Mehrdad Shahn timer and Avinash Vaidheeswaran **National Energy Technology Laboratory 3610 Collins Ferry Road, Morgantown, West Virginia 26505, USA*

(Received 11 December 2020; accepted 23 March 2021; published 12 April 2021)

We present our analysis on microrheology of a bench-scale pulsed fluidized bed, which represents a weakly confined system. Nonlinear gas-particle and particle-particle interactions resulting from pulsed flow are associated with harmonic and subharmonic modes. While periodic structured bubble patterns are observed at the mesoscale, particle-scale measurements reveal anomalous diffusion in the driven granular medium. We use single-particle tracks to analyze ergodicity and ageing properties at two pulsing frequencies having remarkably different mesoscale features. The scaling of ensemble-averaged mean-squared displacement is not unique. The distribution of time-averaged mean-squared displacements is non-Gaussian, asymmetric, and has a finite trivial contribution from particles in crowded quasistatic surroundings. Results indicate weak ergodicity breaking, which along with ageing characterizes the nonstationary and out-of-equilibrium dynamics.

DOI: [10.1103/PhysRevE.103.043103](https://doi.org/10.1103/PhysRevE.103.043103)**I. INTRODUCTION**

Multiphase flows contain a broad range of spatiotemporal scales corresponding to complex nonlinear dynamics [1–6]. Fluidization is a notable example in which particles are suspended by an incoming stream of fluid, whereby they exhibit fluidlike behavior. Traveling kinematic waves manifest as bubbles which create spatial inhomogeneities in solids concentration. In particular, pulsed fluidized beds (PFBs) are characterized by recurring bubble patterns resulting from dynamical structuring and suppression of chaos compared to fluidized beds having nonperturbed inflow. PFBs have shown improved hydrodynamics by reducing or eliminating channeling or clumping of particles and enhanced heat and mass transfer properties while being nonintrusive. Prior studies on PFBs are mostly restricted to meso- and macroscale observations [7–12]. Pulsing excites several interacting modes, and particle-level description is pivotal in elucidating some of the observed features. Trajectories of fluidized particles evolve depending on multiple factors such as external forcing, momentum exchange with carrier phase, interactions with neighbors, material properties, and confinement, and transition through different states. For instance, particles in the vicinity of bubble wakes experience a greater acceleration compared to those near the distributor or other quasistatic regions.

Previous studies [13–17] have examined velocity fluctuations and reported deviations from ideal Brownian motion. The simplistic assumption of Maxwellian distribution breaks down quite easily in multiparticle systems and results in

anomalous diffusion where the ensemble-averaged mean-squared displacement (MSD) is described by

$$\langle x^2(\Delta) \rangle \sim \Delta^\gamma. \quad (1)$$

The process is subdiffusive for $\gamma < 1$ and superdiffusive for $\gamma > 1$, both of which are observed in nature and engineering applications [18–25], while $\gamma = 1$ describes Brownian diffusion. There also exist diffusive environments which cannot be described by a unique value of γ and involve transition of regimes discussed above. Different sources of anomalous diffusion have been studied in the past, which include continuous-time random walk (CTRW), fractional Brownian motion (FBM) and the motion governed by fractional Langevin equation (FLE), scaled Brownian motion (SBM), transport on a fractal support, and heterogeneous diffusion processes (HDP). Previous analyses also include combining these parent processes such as CTRW-FLE [26] and SBM-HDP [27], the latter termed the generalized diffusion process (GDP), where diffusivity follows,

$$D(x, t) \sim (1 + \beta)D_0|x|^\alpha t^\beta. \quad (2)$$

The above equation combines spatial and temporal dependence from the underlying HDP and SBM, respectively. GDP is subdiffusive ($\gamma < 1$) when $\alpha > 2\beta + 4$.

Based on the physics of PFB [10–12,28], we hypothesize the system hosts a combination of parent processes discussed above, as will be shown in the remainder of this article. We also study the effect of ageing, i.e., time lapse after initializing experiments. It must be noted that PFB does not represent confinement in a strict sense. Boundaries or walls are present in the lateral directions which reflect particles after inelastic collisions, while the streamwise transport is constrained by balance between drag exerted by the carrier phase and gravity.

*avinash.vaidheeswaran@netl.doe.gov

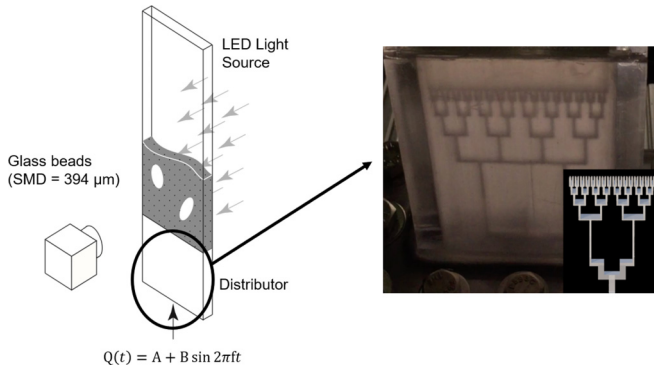


FIG. 1. Schematic of the PFB setup used in this study. The zoomed-in image and inset show the frontal view and a rough sketch of fractal distributor (not drawn to scale).

Hence, we describe the PFB as a weakly confined system. In addition, our unit is quasi-two-dimensional (quasi-2D), since the depth-wise extent is comparable to the size of bubbles, further verified by high-speed videos which reveal their span.

II. EXPERIMENTS

The setup used for experiments (Fig. 1) consists of a bench-scale test section with a cross-sectional area of 50×5 mm. The unit was filled with 18 g of glass particles having a Sauter mean diameter of $394 \mu\text{m}$ and a density of 2.5 g/cm^3 , classified under Geldart group B [29]. The resulting static height was 50 mm. Flow rate at the inlet was pulsed in the form of a sine wave,

$$Q(t) = A + B \sin(2\pi ft), \quad (3)$$

where the base flow rate was $A = 2.6 \text{ l/min}$. The corresponding velocity is higher than the minimum fluidization velocity

U_{mf} , which denotes the minimum velocity required to support the weight of solids. Details regarding the measurement of U_{mf} can be found in Vaidheeswaran *et al.* [30]. The amplitude B is set to 2.1 l/min , and two pulsing frequencies are used, $f = 4$ and 6 Hz . A fractal distributor was 3D printed using a high-precision ultraviolet curing printer. High-speed videos were recorded at 300 Hz over a duration of 20 s using a 120-mm Nikon lens and Fastex IL5L sensor, and the unit was back-lit with an LED light source. The resulting spatial resolution was $0.71 \times 0.71 \text{ mm}$. Glass particles were tracked using an in-house code, PTVRESEARCH [31], based on optical flow equations. Optical distortions were removed using calibrated grid and dewarping [32], and outliers were detected by proper orthogonal decomposition [33]. In a recent effort [34], our method was cross-validated with other particle tracking algorithms when applied to a fluidized bed system, and the predicted velocities compared well. We remark on a few noteworthy limitations of our apparatus. Particle tracks are lost when they enter bubbles, where they become out of focus due to back-lighting. Only particles tracked during the entire duration of our experiments are considered for statistics to avoid unintended bias. Also, the unit is prone to slugging from tight confinement along its depth, which prohibits exploring higher pulsing frequencies and amplitudes as well as using unperturbed flow at the inlet. Further details regarding the experiments can be found in Higham *et al.* [12].

Mesoscale responses to pulsing conditions are shown in Fig. 2. Kinematic waves originate as one-dimensional planar disturbances and transition into structured bubbles as a consequence of interactions between harmonic and subharmonic modes. The recurring patterns are sustained provided their wavelength, λ fit the lateral dimension. Bubbles shift by $\lambda/2$ between successive cycles. We notice λ , associated with bubble size, reduces while changing f from 4 to 6 Hz. At 4 Hz, bubbles are larger and switch sides every half cycle. Wakes

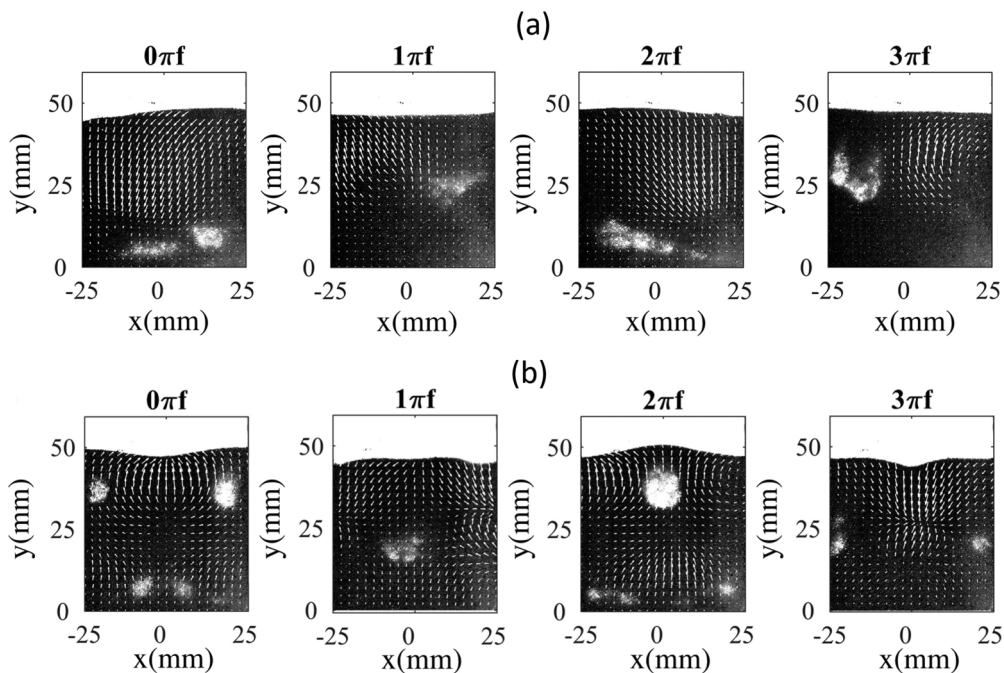
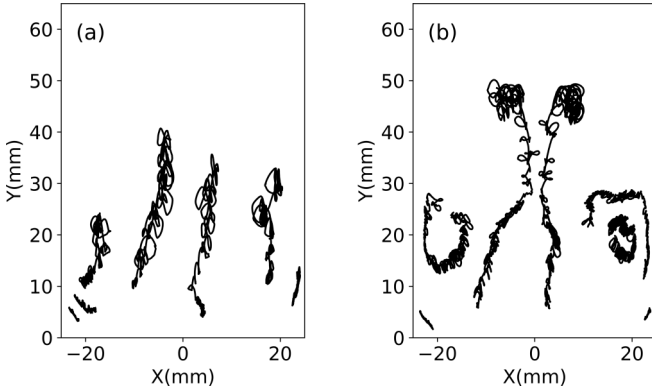


FIG. 2. Structured bubble patterns at (a) $f = 4 \text{ Hz}$ and (b) $f = 6 \text{ Hz}$.


 FIG. 3. Sample trajectories at (a) $f = 4$ Hz and (b) $f = 6$ Hz.

experience a greater compressive stress when defluidized, which makes bubbles less stable and deformed as they propagate upward. The pattern changes to a bubble at the center and two simultaneous bubbles along the walls at 6 Hz, having a smaller size and a more distinct interface.

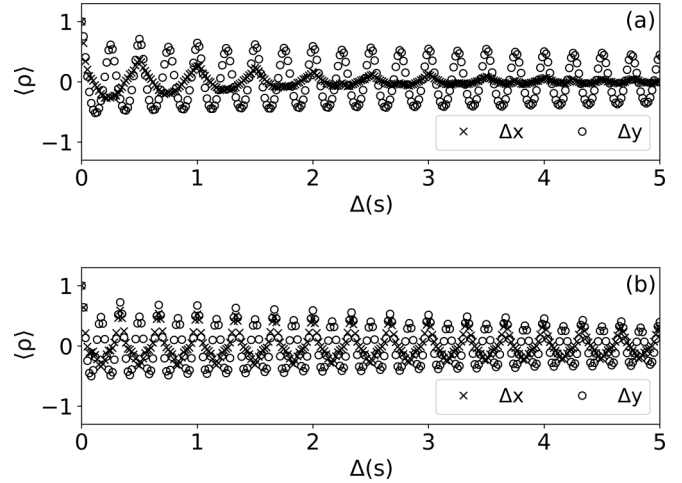
III. RESULTS

Sample trajectories (Fig. 3) indicate nonuniform diffusion in the PFB. We notice a few particles transported over much shorter distances during the entire measurement period. Even if a single-particle track is considered, the motion is altered significantly depending on instantaneous location. Particles in the wake of bubbles take longer steps, while they undergo much shorter displacements in quasistatic regions. Their motion is confined by walls in the lateral direction, and the balance between gravity and interphase drag governs their streamwise transport. The dynamics are strongly coupled to the fluidizing medium, a mechanism neither trivial nor explicitly modeled while describing anomalous diffusion. It is worth mentioning that the effect of drag was included in the generalized Langevin equation [35] to derive kinetic theory, more appropriate for fluidized granular media, albeit continuum modeling efforts have failed to reproduce structured bubbles in PFBs [11]. Stress fields in granular mediums is not adequately represented by the existing frictional models, which is critical to sustain the recurring pattern. We also notice spiral trajectories, possibly due to strongly correlated directional changes [36]. In our case, this is caused by a combination of unidirectional forcing, lateral confines, and preferential movement of bubbles. Momentum transfer from particle interactions is subdued compared to anisotropic wake-induced transport, which breaks the symmetry in turning angle and forms clockwise or counterclockwise patterns close to walls. However, diffusion characteristics vary spatially, and spiraling motion is not present throughout the domain.

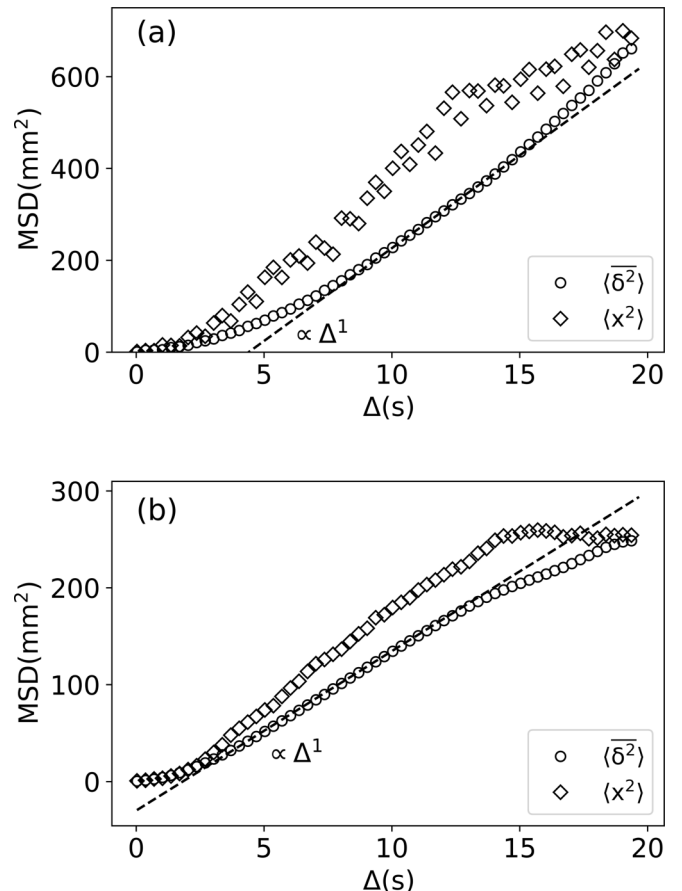
Next we look at autocorrelation, ρ , between displacements in the Cartesian directions. We use the following definition,

$$\rho(\Delta) = \frac{\mathbf{E}[\Delta x_j(t)\Delta x_j(t + \Delta)]}{\sqrt{\text{Var}[\Delta x_j(t)]\text{Var}[\Delta x_j(t + \Delta)]}}, \quad (4)$$

where Δ and Δx_j are lag time and particle displacement. This is ensemble-averaged to obtain $\langle \rho \rangle$ shown in Fig. 4. Again, we notice dominant harmonic and subharmonic responses at both


 FIG. 4. Autocorrelation of displacements, Δx and Δy at (a) $f = 4$ Hz and (b) $f = 6$ Hz.

pulsing frequencies. Lateral steps show a rapid decay of $\langle \rho \rangle$ at $f = 4$ Hz, while the two components reveal comparable persistent memory at $f = 6$ Hz. This occurs in conjunction with redistribution of energy between harmonic and subharmonic modes as explained using proper orthogonal decomposition in our previous study [12]. The long-range correlation observed


 FIG. 5. MSD from experiments at (a) $f = 4$ Hz and (b) $f = 6$ Hz. Dashed lines represent Δ^1 scaling.

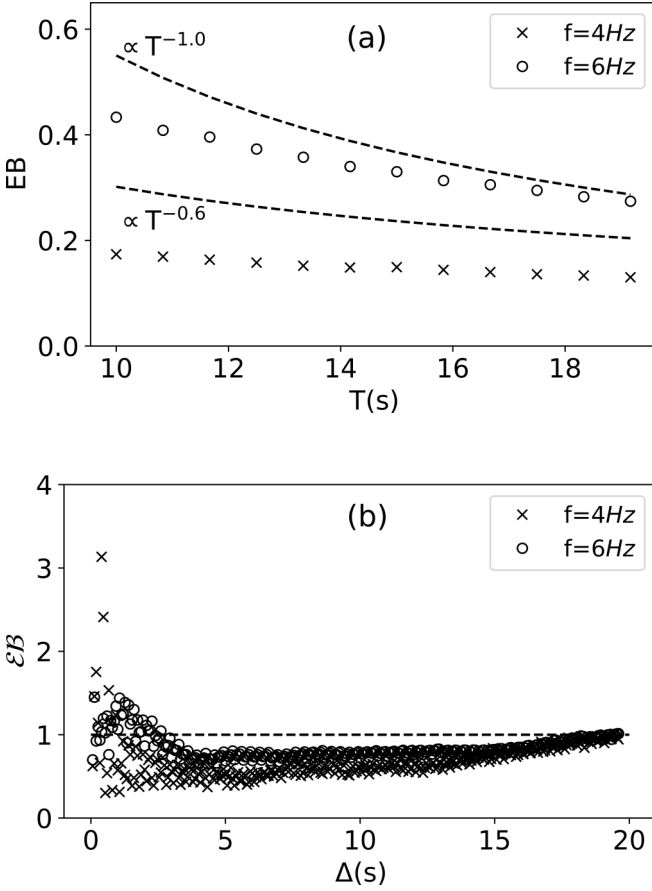


FIG. 6. (a) Ergodicity breaking parameter (EB) vs measurement time (T) at $f = 4$ Hz and 6 Hz, where $\Delta=0.017$ s. Dashed lines represent different slopes for guidance. (b) Variation of alternative ergodic parameter (EB) with lag time (Δ) at $f = 4$ Hz and 6 Hz.

in the collective behavior of particles follows the idea of Kac [37], wherein determinism evolves in multiparticle systems governed by individual stochastic differential equations.

We then examine the behavior of MSD, typically used to study diffusion processes. At this point, ergodicity is not known, and we use two different measures of MSD. First, is the ensemble-averaged MSD, defined as

$$\langle x^2(\Delta) \rangle = \frac{1}{N} \sum_{i=1}^N |x_i(\Delta) - x_i(0)|^2, \quad (5)$$

where N is the total number of tracked particles. The second measure is given by

$$\overline{\langle \delta^2(\Delta) \rangle} = \frac{1}{T - \Delta} \int_0^{T-\Delta} \langle |x(t + \Delta) - x(t)|^2 \rangle dt, \quad (6)$$

which involves both time averaging and ensemble averaging, and T is the total duration of experiments. $\langle x^2 \rangle$ has a nonunique scaling exponent (Fig. 5). Dynamically ordered bubbles result in spatially varying diffusion which may not be apparent while probing the ensemble behavior. $\overline{\langle \delta^2 \rangle}$ has a sublinear exponent initially followed by a crossover to a linear trend at long timescales similar to diffusing insulin granules [38]. More tracked particles participate in wake transport over longer periods. Propagation of bubbles separates such

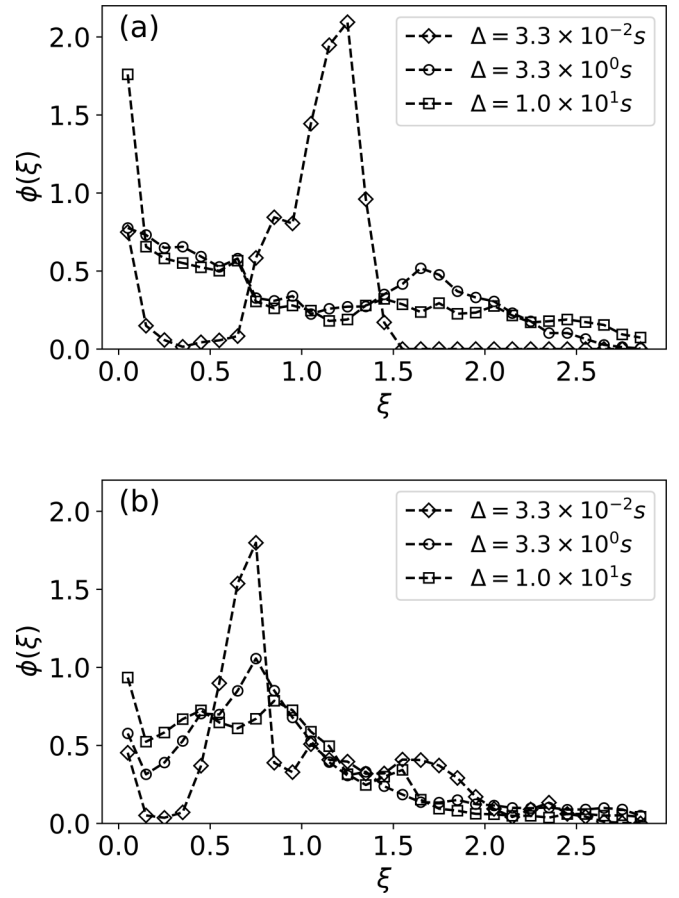


FIG. 7. Amplitude scatter distribution $\phi(\xi)$ at (a) $f = 4$ Hz and (b) 6 Hz.

entrained particles from crowded surroundings, and their displacements become increasingly uncorrelated in time. This could cause an antipersistent motion leading to subdiffusion at short timescales with a gradual transition to memoryless diffusion typical of a CTRW. The final crossover to $\sim \Delta^0$ for $\Delta \rightarrow T$ is due to confinement as reported for GDPs and SBMs [27,39], in contrast to purely subdiffusive CTRWs, where plateaus are not present for time-averaged MSDs. Detailed measurements such as turning-angle distributions [36,40,41] may be required to formulate a model describing these trends in $\langle x^2 \rangle$ and $\langle \delta^2 \rangle$.

Besides, we notice significant difference in scaling between $\langle x^2 \rangle$ and $\langle \delta^2 \rangle$, indicating weak nonergodicity [39,42–44]. This eliminates the possibility of ensemble diffusion in PFB governed by transport on a fractal support, which is ergodic by definition. $\langle x^2 \rangle$ and $\overline{\langle \delta^2 \rangle}$ show the same limiting behavior at $\Delta/T \rightarrow 0$ and $\Delta/T \rightarrow 1$. The latter is apparent from Eq. (6), which has a singularity for $\Delta \rightarrow T$, thus placing the constraint, $\langle x^2 \rangle = \overline{\langle \delta^2 \rangle}$. Also, the linear scaling in $\overline{\langle \delta^2 \rangle}$ is prevalent for an appreciable period at both values of f , previously observed for sub- and superdiffusive unconfined HDPs [39]. This might lead to a false impression of Brownian motion unless supported by complementary statistical measures.

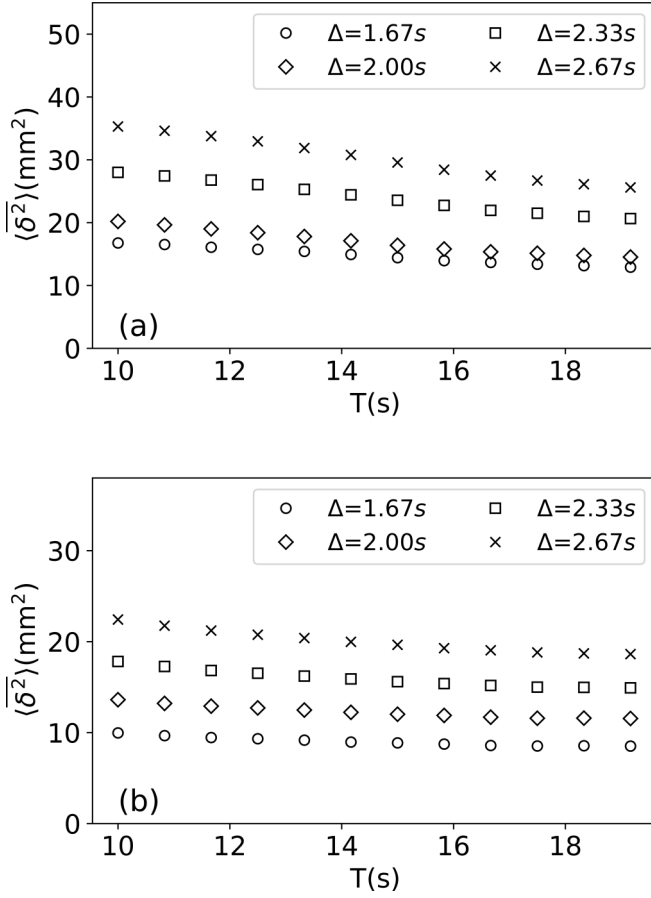


FIG. 8. Variation of time-averaged MSD $\langle \delta^2 \rangle$ with measurement time (T) at (a) $f = 4$ Hz and (b) $f = 6$ Hz.

To elucidate nonergodic dynamics in PFB, we define the ergodicity-breaking parameter (EB) as

$$\text{EB}(\Delta) = \frac{\overline{\langle \delta^2(\Delta) \rangle^2}}{\langle \delta^2(\Delta) \rangle^2} - 1. \quad (7)$$

EB represents dispersion in $\overline{\delta^2}$, and we examine its variation with T to identify deviation from ergodic behavior. EB for a Brownian motion follows $\lim_{\Delta/T \rightarrow 0} \text{EB}_{\text{BM}}(\Delta) = \frac{4}{3} \frac{\Delta}{T}$, indicated by the curve $\propto T^{-1}$ in Fig. 6. We observe a more gradual change in EB approaching a finite value for $\Delta/T \rightarrow 0$ as reported for anomalous stochastic processes governed by HDPs and CTRWs [45]. To further investigate the nature of ergodicity breaking, we use an alternative ergodic parameter EB following the definition of Godec and Metzler [46], given by

$$\text{EB}(\Delta) = \frac{\overline{\langle \delta^2(\Delta) \rangle}}{\langle x^2(\Delta) \rangle}. \quad (8)$$

At short timescales, there is a pronounced scatter in EB. Particles reside in a given state for a duration determined by the spatiotemporal evolution of the system. As measurement time increases, more particles transition between states and the change in EB becomes more moderate. We notice $\text{EB} \neq 1$ at intermediate timescales, confirming deviation from ergodic dynamics. We also find $\text{EB} = 1$ for $\Delta/T \rightarrow 1$ due to

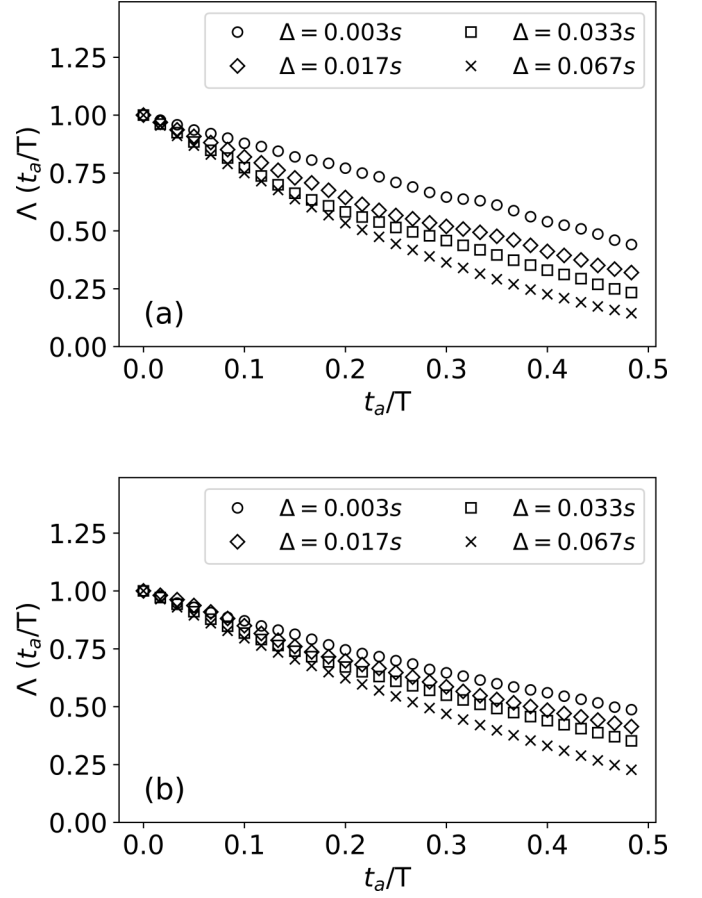


FIG. 9. Variation of ageing factor (Λ) with dimensionless ageing time (t_a/T) at (a) $f = 4$ Hz and (b) $f = 6$ Hz for different values of Δ as indicated.

confinement, which is not indicative of ergodicity though it mathematically represents a necessary condition. A sufficient condition for ergodicity is $\text{EB} \rightarrow 0$ for $\Delta/T \rightarrow 0$, which is clearly not satisfied here.

In addition, we examine the spread in $\overline{\delta^2}$ (Fig. 7) using the nondimensional parameter ξ , defined as

$$\xi = \frac{\overline{\langle \delta^2(\Delta) \rangle}}{\langle \delta^2(\Delta) \rangle}. \quad (9)$$

The distribution $\phi(\xi)$ is Gaussian centered at 1 ($\xi = 1$ represents ergodicity) for a Brownian walker. For $\Delta/T \ll 1$, $\phi(\xi)$ has distinct peaks at $\xi > 1$ ($f = 4$ Hz) and $\xi < 1$ ($f = 6$ Hz). We notice a significant scatter in ξ for growing lag times while deviating from ergodic dynamics. $\phi(\xi)$ is finite at $\xi = 0$ for all values of Δ , as observed for subdiffusive CTRWs [47]. The contribution from quasistatic particles is more prominent for longer lag times at $f = 4$ Hz. These findings corroborate combination of parent stochastic processes dictating the underlying anomalous diffusion. Weak ergodicity breaking essentially results from information content in single-particle trajectories which are not retained while ensemble averaging. Besides, wake transport is not truly reproducible, and distances over which it occurs could vary, leading to nonequilibrium relaxation.

Finally we look at ageing characteristics, which along with ergodicity breaking determine the (non-)stationary nature of a stochastic process. $\langle \overline{\delta^2} \rangle$ shows a monotonic drop as a function of T (Fig. 8) for different values of Δ . This is indicative of a collective subdiffusive anomalous process. Analogous ageing behavior in a subdiffusive environment is found in other instances, including plasma membranes [23] and fibrin matrices [48]. As a consequence, the system appears less diffusive as it evolves longer. More and more particles transition through quasistatic regions which overpopulate the tails of wait-time distributions. If the on-off response of particles switching between wake transport and interaction with neighbors (through friction and collision) is considered, the occurrence and duration of these events appear random at short timescales. Upon prolonged measurements, occasionally long on and off states are obtained, characteristic of nonstationary and out-of-equilibrium dynamics [49,50]. This in essence results in the observed ageing behavior. But individual motion of particles could vary depending on localized states. We further quantify the ensemble behavior using ageing factor [39] defined as

$$\Lambda(t_a, \Delta) = \frac{\langle \overline{\delta_a^2(\Delta)} \rangle}{\langle \overline{\delta^2(\Delta)} \rangle}, \quad (10)$$

where $\overline{\delta_a^2}$ refers to the time-averaged MSD considering the ageing time, t_a , given by

$$\overline{\delta_a^2(t_a)} = \frac{1}{T - \Delta - t_a} \int_{t_a}^{T-\Delta} \langle |x_i(t + \Delta) - x_i(t)|^2 \rangle dt. \quad (11)$$

The above expression is ensemble averaged while calculating Λ for different values of t_a shown in Fig. 9. There

is a steady drop in Λ even for $\Delta/T \ll 1$ due to continued localization of particles in quasistatic regions, again indicative of subdiffusive behavior. Even though the mesoscale response (bubble pattern) is completely different at $f = 4$ and 6 Hz, similar anomalous diffusion characteristics are observed.

IV. CONCLUSION

We analyzed anomalous diffusion in PFB having a spatiotemporal dependence using single-particle tracking and found traits from a combination of parent stochastic processes. PFB represents a driven granular system having complex nonlinear interactions. Finite memory or long-range correlations stem from individual stochastic motions, in line with the ideas of Kac surrounding propagation of chaos [37]. Time-averaged and ensemble-averaged MSDs deviate indicating weak ergodicity breaking. MSDs approach a plateau similar to constrained GDPs or SBMs, although our setup is weakly confined wherein the streamwise transport is balanced between interphase drag and gravity. The distribution of amplitude scatter is wide, non-Gaussian, asymmetric, and has a finite contribution at zero stemming from particles in quasistatic surroundings, a feature prevalent in CTRWs. The system also exhibits ageing as more traps are encountered over a prolonged duration. The ageing factor decays monotonically, suggesting an overall subdiffusive process at the two pulsing frequencies having a different mesoscale response altogether. We expect structured flow patterns in PFBs while lowering the effective diffusivity compared to fluidized media having an unperturbed inflow, which needs to be verified.

-
- [1] G.-B. Zhao and Y.-R. Yang, Multiscale resolution of fluidized-bed pressure fluctuations, *AIChE J.* **49**, 869 (2003).
 - [2] P. Blomgren, A. Palacios, B. Zhu, S. Daw, C. Finney, J. Halow, and S. Pannala, Bifurcation analysis of bubble dynamics in fluidized beds, *Chaos* **17**, 013120 (2007).
 - [3] W. D. Fullmer and C. M. Hrenya, The clustering instability in rapid granular and gas-solid flows, *Annu. Rev. Fluid Mech.* **49**, 485 (2017).
 - [4] A. Vaidheeswaran and M. Lopez de Bertodano, Stability and convergence of computational eulerian two-fluid model for a bubble plume, *Chem. Eng. Sci.* **160**, 210 (2017).
 - [5] A. Vaidheeswaran, A. Clausse, W. D. Fullmer, R. Marino, and M. Lopez de Bertodano, Chaos in wavy-stratified fluid-fluid flow, *Chaos* **29**, 033121 (2019).
 - [6] A. Vaidheeswaran and S. Rowan, Chaos and recurrence analyses of pressure signals from bubbling fluidized beds, *Chaos, Solitons & Fractals* **142**, 110354 (2021).
 - [7] D. V. Pence and D. E. Beasley, Chaos suppression in gas-solid fluidization, *Chaos* **8**, 514 (1998).
 - [8] M.-O. Coppens and J. R. van Ommen, Structuring chaotic fluidized beds, *Chem. Eng. J.* **96**, 117 (2003).
 - [9] B. Hadi, J. R. van Ommen, and M.-O. Coppens, Enhanced particle mixing in pulsed fluidized beds and the effect of internals, *Ind. Eng. Chem. Res.* **51**, 1713 (2012).
 - [10] K. Wu, L. de Martín, and M.-O. Coppens, Pattern formation in pulsed gas-solid fluidized beds—the role of granular solid mechanics, *Chem. Eng. J.* **329**, 4 (2017).
 - [11] L. de Martín, C. Ottevanger, J. R. van Ommen, and M.-O. Coppens, Universal stability curve for pattern formation in pulsed gas-solid fluidized beds of sandlike particles, *Phys. Rev. Fluids* **3**, 034303 (2018).
 - [12] J. E. Higham, M. Shahnam, and A. Vaidheeswaran, Using a proper orthogonal decomposition to elucidate features in granular flows, *Granular Matter* **22**, 86 (2020).
 - [13] T. P. C. van Noije and M. H. Ernst, Velocity distributions in homogeneous granular fluids: The free and the heated case, *Granular Matter* **1**, 57 (1998).
 - [14] A. Barrat, T. Biben, Z. Rácz, E. Trizac, and F. Van Wijland, On the velocity distributions of the one-dimensional inelastic gas, *J. Phys. A: Math. Gen.* **35**, 463 (2002).
 - [15] E. Ben-Naim and J. Machta, Stationary States and Energy Cascades in Inelastic Gases, *Phys. Rev. Lett.* **94**, 138001 (2005).
 - [16] S. Moka and P. R. Nott, Statistics of Particle Velocities in Dense Granular Flows, *Phys. Rev. Lett.* **95**, 068003 (2005).
 - [17] A. Vaidheeswaran, F. Shaffer, and B. Gopalan, Statistics of velocity fluctuations of Geldart A particles in a circulating fluidized bed riser, *Phys. Rev. Fluids* **2**, 112301(R) (2017).
 - [18] T. H. Solomon, E. R. Weeks, and H. L. Swinney, Observation of Anomalous Diffusion and Lévy Flights in a

- Two-Dimensional Rotating Flow, *Phys. Rev. Lett.* **71**, 3975 (1993).
- [19] I. Y. Wong, M. L. Gardel, D. R. Reichman, E. R. Weeks, M. T. Valentine, A. R. Bausch, and D. A. Weitz, Anomalous Diffusion Probes Microstructure Dynamics of Entangled F-Actin Networks, *Phys. Rev. Lett.* **92**, 178101 (2004).
- [20] X. S. Xie, P. J. Choi, G.-W. Li, N. K. Lee, and G. Lia, Single-molecule approach to molecular biology in living bacterial cells, *Annu. Rev. Biophys.* **37**, 417 (2008).
- [21] J. Mattsson, H. Wyss, A. Fernandez-Nieves, K. Miyazaki, Z. Hu, D. Reichman, and D. Weitz, Soft colloids make strong glasses, *Nature* **462**, 83 (2009).
- [22] I. Bronstein, Y. Israel, E. Kepten, S. Mai, Y. Shav-Tal, E. Barkai, and Y. Garini, Transient Anomalous Diffusion of Telomeres in the Nucleus of Mammalian Cells, *Phys. Rev. Lett.* **103**, 018102 (2009).
- [23] A. V. Weigel, B. Simon, M. M. Tamkun, and D. Krapf, Ergodic and nonergodic processes coexist in the plasma membrane as observed by single-molecule tracking, *Proc. Natl. Acad. Sci. USA*, **108**, 6438 (2011).
- [24] G. R. Kneller, K. Baczynski, and M. Pasenkiewicz-Gierula, Communication: Consistent picture of lateral subdiffusion in lipid bilayers: Molecular dynamics simulation and exact results, *J. Chem. Phys.* **135**, 141105 (2011).
- [25] M. Palombo, A. Gabrielli, V.D.P. Servedio, G. Ruocco, and S. Capuani, Structural disorder and anomalous diffusion in random packing of spheres, *Sci. Rep.* **3**, 2631 (2013).
- [26] J. H. P. Schulz, E. Barkai, and R. Metzler, Aging Renewal Theory and Application to Random Walks, *Phys. Rev. X* **4**, 011028 (2014).
- [27] A. G. Cherstvy and R. Metzler, Ergodicity breaking, ageing, and confinement in generalized diffusion processes with position and time dependent diffusivity, *J. Stat. Mech.* (2015) P05010.
- [28] V. Francia, K. Wu, and M.-O. Coppens, Dynamically structured fluidization: Oscillating the gas flow and other opportunities to intensify gas-solid fluidized bed operation, *Chem. Eng. Process.* **159**, 108143 (2021).
- [29] D. Geldart, Types of gas fluidization, *Powder Technol.* **7**, 285 (1973).
- [30] A. Vaidheeswaran, R. Pandey, M. A. Clarke, H. Ashfaq, and W. A. Rogers, Fluidization of Group A Glass Particles: Experiments and Preliminary Validation, Technical Report Series, National Energy Technology Laboratory DOE/NETL-2020/2135 (National Energy Technology Laboratory, 2020).
- [31] W. D. Fullmer, J. E. Higham, C. Q. LaMarche, A. Issangya, R. Cocco, and C. M. Hrenya, Comparison of velocimetry methods for horizontal air jets in a semicircular fluidized bed of geldart group D particles, *Powder Technol.* **359**, 323 (2020).
- [32] J. E. Higham and W. Brevis, When, what and how image transformation techniques should be used to reduce error in particle image velocimetry data? *Flow Meas. Instrum.* **66**, 79 (2019).
- [33] J. E. Higham, W. Brevis, and C. J. Keylock, A rapid non-iterative proper orthogonal decomposition based outlier detection and correction for PIV data, *Meas. Sci. Technol.* **27**, 125303 (2016).
- [34] J. Weber, J. E. Higham, J. Musser, and W. D. Fullmer, Critical analysis of velocimetry methods for particulate flows from synthetic data, *Chem. Eng. J.* **415**, 129032 (2021).
- [35] V. Garzó, S. Tenneti, S. Subramaniam, and C. M. Hrenya, Enskog kinetic theory for monodisperse gas-solid flows, *J. Fluid Mech.* **712**, 129 (2012).
- [36] Z. Sadjadi, M. R. Shaebani, H. Rieger, and L. Santen, Persistent-random-walk approach to anomalous transport of self-propelled particles, *Phys. Rev. E* **91**, 062715 (2015).
- [37] M. Kac, Foundations of kinetic theory, in *Proceedings of the Third Berkeley Symposium on Mathematical Statistics and Probability* (University of California Press, Berkeley and Los Angeles, 1956), Vol. 3, pp. 171–197.
- [38] S. M. A. Tabei, S. Burov, H. Y. Kim, A. Kuznetsov, T. Huynh, J. Jureller, L. H. Philipson, A. R. Dinner, and N. F. Scherer, Intracellular transport of insulin granules is a subordinated random walk, *Proc. Natl. Acad. Sci. USA* **110**, 4911 (2013).
- [39] R. Metzler, J.-H. Jeon, A. G. Cherstvy, and E. Barkai, Anomalous diffusion models and their properties: Non-stationarity, non-ergodicity, and ageing at the centenary of single particle tracking, *Phys. Chem. Chem. Phys.* **16**, 24128 (2014).
- [40] M. R. Shaebani, Z. Sadjadi, I. M. Sokolov, H. Rieger, and L. Santen, Anomalous diffusion of self-propelled particles in directed random environments, *Phys. Rev. E* **90**, 030701(R) (2014).
- [41] M. R. Shaebani and H. Rieger, Transient anomalous diffusion in run-and-tumble dynamics, *Front. Phys.* **7**, 120 (2019).
- [42] G. Bel and E. Barkai, Weak Ergodicity Breaking in the Continuous-Time Random Walk, *Phys. Rev. Lett.* **94**, 240602 (2005).
- [43] M. A. Lomholt, I. M. Zaid, and R. Metzler, Subdiffusion and Weak Ergodicity Breaking in the Presence of a Reactive Boundary, *Phys. Rev. Lett.* **98**, 200603 (2007).
- [44] I. M. Sokolov, Models of anomalous diffusion in crowded environments, *Soft Matter* **8**, 9043 (2012).
- [45] A. G. Cherstvy and R. Metzler, Ergodicity breaking and particle spreading in noisy heterogeneous diffusion processes, *J. Chem. Phys.* **142**, 144105 (2015).
- [46] A. Godec and R. Metzler, Finite-Time Effects and Ultraweak Ergodicity Breaking in Superdiffusive Dynamics, *Phys. Rev. Lett.* **110**, 020603 (2013).
- [47] A. G. Cherstvy, A. V. Chechkin, and R. Metzler, Anomalous diffusion and ergodicity breaking in heterogeneous diffusion processes, *New J. Phys.* **15**, 083039 (2013).
- [48] R. R. L. Aure, C. C. Bernido, M. V. Carpio-Bernido, and R. G. Bacabac, Damped white noise diffusion with memory for diffusing microprobes in ageing fibrin gels, *Biophys. J.* **117**, 1029 (2019).
- [49] E. M. Bertin and J.-P. Bouchaud, Linear and nonlinear response in the aging regime of the one-dimensional trap model, *Phys. Rev. E* **67**, 065105(R) (2003).
- [50] S. Burov and E. Barkai, Occupation Time Statistics in the Quenched Trap Model, *Phys. Rev. Lett.* **98**, 250601 (2007).